doi:10.1093/jmcb/mjy005

Article

Egg CD9 protein tides correlated with sperm oscillations tune the gamete fusion ability in mammal

Benjamin Ravaux, Sophie Favier, Eric Perez, and Christine Gourier*

Laboratoire de Physique Statistique, Ecole Normale Superieure/PSL Research University, UPMC Univ Paris 06, Université Paris Diderot, CNRS, 75005 Paris, France
* Correspondence to: Christine Gourier, E-mail: gourier@lps.ens.fr

Edited by Qi Zhou

Mammalian fertilization involves membrane events—adhesion, fusion, sperm engulfment, membrane block to polyspermy—whose causes remain largely unknown. Recently, specific oscillations of the sperm in contact with the egg were shown to be necessary for fusion. Using a microfluidic chip to impose the venue for the encounter of two gametes allowed real-time observation of the membrane remodelling occurring at the sperm/egg interface. The spatiotemporal mapping of egg CD9 revealed that this protein concentrates at the egg/sperm interface as a result of sperm oscillations, until a CD9-rich platform is nucleated on which fusion immediately takes place. Within 2–5 min after fusion, most of the CD9 leaves the egg for the external aqueous medium. Then an egg membrane wave engulfs the sperm head in ~25 min. These results show that sperm oscillations initiate the CD9 recruitment that causes gamete fusion after which CD9 and associated proteins leave the membrane in a process likely to contribute to block polyspermy. They highlight that the gamete fusion story in mammals is an unexpected interplay between mechanical constraints and proteins.

Keywords: mammalian fertilization, membrane dynamics, real-time imaging, CD9, sperm oscillations, gamete fusion

Introduction

Within the course of mammalian fertilization, gamete fusion is the culmination of a membrane interaction process begun at the onset of sperm and egg contact after the fertilizing sperm has successfully crossed the zona pellucida (ZP) (Evans, 2012). The membrane events that take place at the gamete interface during this prefusional membrane interacting period are poorly known. They involve three proteins—CD9 and Juno on the egg, Izumo1 on the sperm—and one specific flagellum beating mode, which are the only currently known factors mandatory for fusion in mammals (Kaji et al., 2000; Le Naour et al., 2000; Miyado et al., 2000; Inoue et al., 2005; Bianchi et al., 2014; Ravaux et al., 2016). Juno and Izumo1 are adhesion proteins that form a ligand/receptor pair able to generate a robust cell adhesion (Bianchi et al., 2014; Chalbi et al., 2014; Inoue et al., 2015). CD9 tetraspanin is a membrane organizer (Boucheix and Rubinstein, 2001; Hemler, 2005) that gathers on the egg membrane several sperm receptors in evenly distributed nanodomains on which sperm can strongly bind upon its onset of contact with the egg (Jegou et al., 2011). CD9 is also suspected to control microvilli shape (Runge et al., 2007; Zylkiewicz et al., 2010), a parameter that can be determinant for fusion (Chernomordik et al., 2006). As for flagellum beating, it imposes the sperm head up and down oscillations on the egg membrane that generate mechanical constraints on the underlying microvilli (Ravaux et al., 2016). The way in which these elements contribute during the early minutes of a sperm and egg encounter to control gamete fusion and conversely whether they may combine within the early minutes after the fusion reaction to favour sperm internalization and limit the chances that another sperm fuse and lead to unviable polyspermy are still a mystery.

To tackle these questions, we imaged in real time during dozens of minutes, from the onset of contact of the gametes, the egg membrane in the sperm/egg contact zone. The technical barrier of the unpredictable location of the fertilizing sperm in the extended egg surface was lifted by using a recently developed microfluidic device that maintained the oocyte still in a tailored egg-cup, and that guided a single fertilizing sperm to a

Received August 17, 2017. Revised January 17, 2018. Accepted January 21, 2018.

predefined portion of the egg membrane located in the focal plane of a microscope (Ravaux et al., 2016). Bright field and confocal time-lapse imaging were combined to simultaneously follow with submicrometric and 20 sec resolutions (i) the topological remodelling of the egg membrane, (ii) the spatiotemporal evolution of egg CD9 distribution, and (iii) the spatiotemporal transfer of a nuclear dye from the egg cytoplasm to the sperm DNA.

This unprecedented time-lapse observation allowed to describe the kinetics of the topological and CD9 membrane remodellings taking place during the early phases of fertilization. They also allowed to discriminate the membrane events due to sperm/egg interaction and leading to membrane fusion from those resulting from fusion and potentially involved in polyspermy block or other post-fusion processes. This study revealed the causal link between the specific oscillation of the sperm head on the egg membrane and a densification of CD9 at the sperm/egg interface leading in a few dozens of seconds to CD9-dense platforms. The fusion reaction strictly coincides in space and time with the nucleation of the first CD9-dense platform that specifically faces the sperm equatorial segment. Immediately after fusion, CD9 leaves the contact zone, followed within a few minutes by the sudden release of more than 50% of CD9 from the whole oolemma in a process susceptible to contribute to a polyspermy block. In the meantime, an egg membrane wave starts to spread above the sperm head and progressively engulfs it. After 25 min, when sperm internalization is complete, membrane excess buds from the fusion place and detaches as a few micrometre-sized vesicles.

Results

Egg CD9 densification, depletion, and release during the early minutes of sperm/egg encounter

To tackle the dynamics of egg CD9 during the early phases of mammalian fertilization, we performed individual *in vitro* fertilization (IIVF) assays in a microfluidic chip. For each assay, one single acrosome-reacted spermatozoon was guided to a predefined egg membrane portion (<2% of the total egg surface) of a ZP-free CD9-EGFP oocyte preloaded with a nuclear dye (Hoechst) and let free to interact with it. Confocal time-lapse microscopy allowed to image in real-time the sperm/egg encounter and subsequent membrane remodelling in the region of gamete interface with the best front view during dozens of minutes. The spatiotemporal membrane evolution of egg CD9 and that of Hoechst nuclear dye transfer to the sperm DNA were simultaneously quantified (Figure 1). Successful fertilizations systematically showed a sequence of three phases for CD9: (i) from sperm/egg encounter to membrane fusion (2–4 min depending on the gamete couple), CD9 accumulates at the gamete interface (Figures 1B and 2A; Supplementary Figures S1A and S2A); (ii) immediately after the fusion reaction, CD9 leaves the sperm/egg contact zone in a process that lasts for ~2 min (Figures 1B and 2B; Supplementary Figures S1A and S2A); (iii) a few minutes after fusion (2–5 min depending on the gamete couple), a sudden release of CD9 from the whole membrane in the surrounding medium takes place (Figures 1C, D and 2C; Supplementary Figures S1B and S2B), decreasing the CD9 membrane amount by more than half (Figure 1C).

A specific flagellum beating mode is required for CD9 recruitment at the sperm/egg interface

Consistent with the previous results (Ravaux et al., 2016), acrosome-reacted sperm interacting with CD9-EGFP egg membrane were shown to display three different modes of flagellum beating: (i) vigorous whiplash movement (Table 1, Group 1), (ii) small amplitude flagellum oscillations (Table 1, Group 2), and (iii) vigorous oscillations perpendicularly to the egg membrane (Table 1, Group 3). Note that these flagellum beating modes observed here without the influence of the ZP are still relevant in physiological condition. Indeed, we have inseminated ZP intact CD9-KO oocytes (N = 40) with wild-type sperm and we have observed the oscillations of the sperm cells interacting with the eggs (N = 82) in the perivitelin space. Even though the amplitude of flagellum beating was limited by the presence of the ZP, the three modes of oscillations could be observed (Supplementary Videos S1–S3) with a prevalence of Group 3 (45%) and Group 2 (39%) types.

During IIVF assays on ZP-free CD9-EGFP eggs in the microfluidic chip, we observed that with spermatozoa from Group 1, the egg membrane portion swept by the sperm head was rapidly losing its fluorescence while fluorescence was transferring on the sperm head (Supplementary Figure S3A), suggesting that membrane fragments were extracted from the egg membrane and stuck to the sperm head upon its brutal tangential rotation. In the case of sperm from Group 2, its interaction with the egg membrane did not influence the distribution of CD9-EGFP (Supplementary Figure S3B). An increase of CD9 concentration in the sperm/egg contact area was exclusively occurring on oocytes in interaction with sperm from Group 3 and in the absence of Juno antibody known to prevent Izumo1/Juno intercellular bonds (Table 1, Figure 2A; Supplementary Figures S1A, S2A, and S3C).

CD9 accumulation leads to the nucleation of a CD9-enriched platform on which gamete fusion immediately takes place if located in the sperm/equatorial segment area

The IIVF assays revealed that sperm/egg fusion was systematically preceded by the recruitment of egg CD9 in the contact zone suggesting a causal relation between CD9 recruitment and membrane fusion. In return, CD9 recruitment was mostly but not always followed by membrane fusion. It happened in one case (over five) that a CD9 recruitment occurred without leading to fusion (Table 1 and Supplementary Figure S3C). To further investigate the correlation between CD9 recruitment and membrane fusion, we established in the cases of successful (Figure 3A–C) and unsuccessful fusion (Figure 3D–F) the spatiotemporal mapping of both CD9 and Hoechst nuclear dyes densities over a line crossing the three regions of the spermatozoon head: post-acrosomal, equatorial and the post-equatorial (Figure 3A and D). These sperm regions are not equivalent regarding membrane fusion and the equatorial region is described as the place where gamete fusion is initiated (Yanagimachi and Noda, 1970; Bedford et al., 1979; Yanagimachi, 1994). Interestingly, in the case where

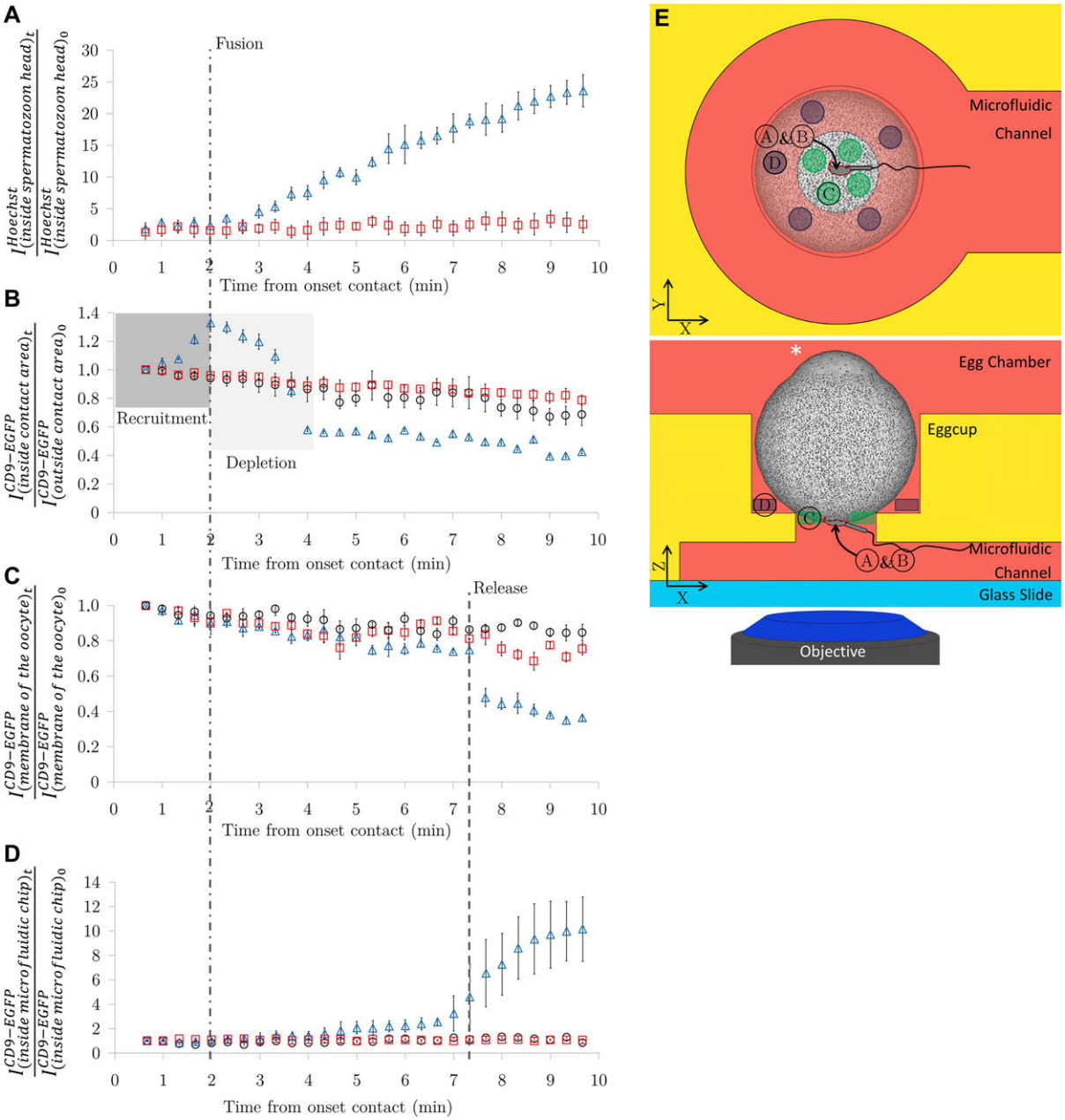

Figure 1 Dynamics of egg CD9 and nuclear dye transfer during the early phases of fertilization in mouse. Each curve of this figure corresponds to intensities collected on one single experiment illustrative of (i) successful fertilizations (blue triangles), (ii) failed fertilizations (red squares, control 1), (iii) absence of sperm (black circles, control 2). The same three illustrative experiments were kept over the four graphs in order to highlight the strict concomitance of (i) flagellum beating phase and CD9 influx at the sperm/egg interface (dark grey box), (ii) onset of fusion (vertical dashed line) and abrupt transition from CD9 influx (dark grey box) to CD9 withdrawal (light grey box) from the sperm/egg interface, and (iii) collapse of CD9 amount from the whole egg membrane and sudden arrival of CD9 in the nearby environment of the egg (vertical line). (**A**) Time evolution of Hoechst nuclear dye transfer from egg cytoplasm to sperm DNA. (**B**) Time evolution of CD9-EGFP at the sperm/egg interface. For **A** and **B**, fluorescence intensities were quantified in a ROI delimitated by a freehand drawing outline of the sperm head on the egg membrane (sperm/egg interface). For each acquisition time, the drawing of such ROI was repeated five times providing five independent CD9-EGFP mean density values. Each data point corresponds to the average of these five values normalized by the intensity measured at the onset of contact time (t = 0). The error bars correspond to their standard error. (**C**) Time evolution of egg CD9-EGFP at the egg membrane outside the sperm/egg interface. For each acquisition time, five circular ROI of 5 µm diameter were evenly drawn at the egg membrane, outside the sperm/egg interface, providing five CD9-EGFP mean density values. Each data point corresponds to the average of these five values normalized by the intensity measured in the same ROI at the onset of contact time. The error bars correspond to their standard error. (**D**) Time evolution of egg CD9-EGFP in the medium surrounding the egg. The same protocol as for **C** was applied except that the five circular ROI were taken outside the egg and not on the egg membrane. (**E**) Microcfluidic device and location of the ROI used in **A**–**D**.

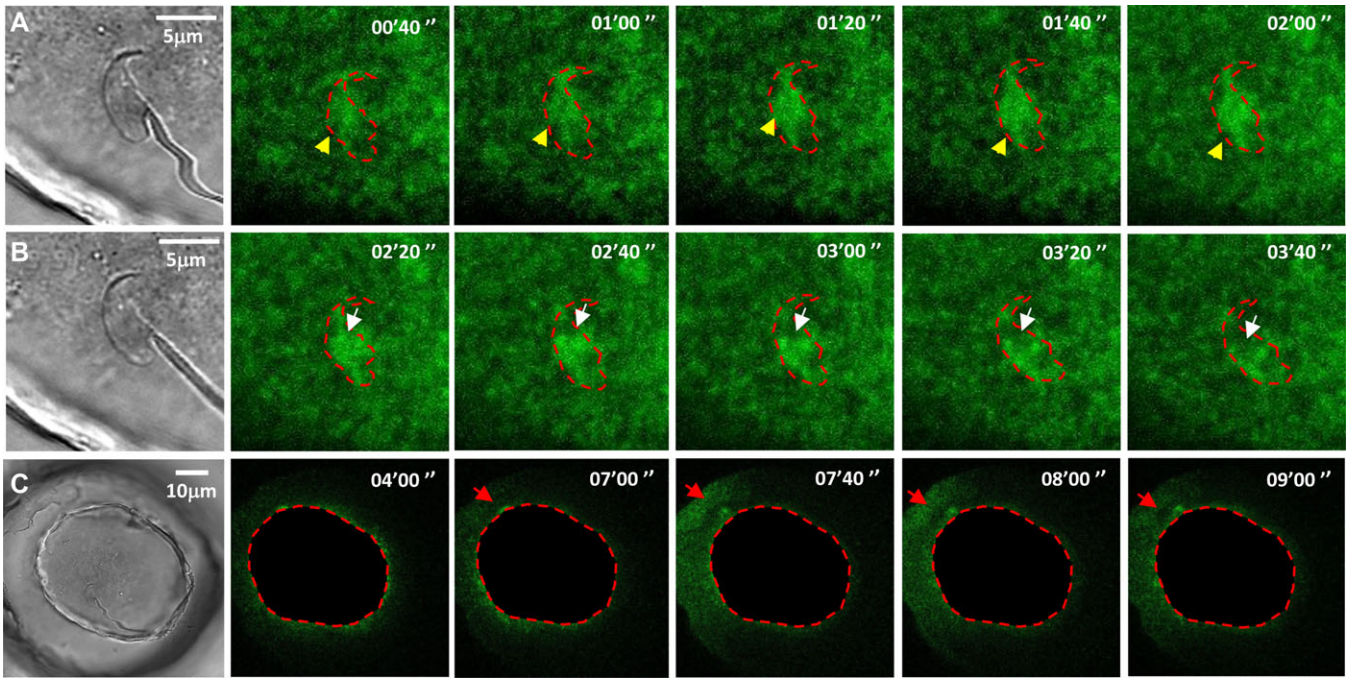

Figure 2 Dynamics of CD9-EGFP during successful IIVF. (**A**) Recruitment of CD9-EGFP (yellow arrow) in the sperm/egg interface (dashed red line contour) before the gamete fusion reaction. (**B**) Depletion of CD9-EGFP (white arrow) from the contact area after gamete fusion. (**C**) Release of CD9-EGFP in the egg surrounding medium (red arrow) a few minutes after gamete fusion. The black mask with red-dashed contours hides the fluorescence of the egg membrane to better reveal CD9-EGFP outside the egg. The timer gives the time from the onset of the gamete contact.

Table 1 CD9 recruitment, depletion, release, and fertilizing status of couples of gametes interaction and the membrane level as a function of flagellum beating.

Flagellum beating mode	Number of sperm/egg couples	CD9 recruitment		Fusion	CD9 depletion	CD9 release	Vesicle budding
		Equatorial segment	Post-acrosomal segment				
Group 1	3	0	0	0	3	0	0
Group 2	7	0	0	0	0	0	0
Group 3	8	4[a]	1	4[a]	4[a]	4[a]	2[a]
Group 3 + Juno Ab	7	0	0	0	0	0	0

[a]Gametes that fuse are those on which CD9 concentrates in the equatorial segment.

a densification without fusion was observed, CD9 did not concentrate in the equatorial area. Instead, it mainly concentrated in the acrosomal area (Figure 3E; Supplementary Figure S3A) and stayed there, with some dense CD9 spots nucleated in this region. The absence of Hoechst signal in the associated map (Figure 3F) confirmed the absence of fusion. By contrast, for successful fertilizations, CD9 recruitment was taking place over the three regions of the spermatozoon head with higher concentration in the equatorial segment (Figure 3B). CD9 density culminated there, 120 sec after gamete contact in the given example, in a micrometre-sized enriched platform on which membrane fusion immediately took place as attested by the perfect spatial and temporal coincidence with the Hoechst appearance (Figure 3C).

CD9 and topological egg membrane remodellings after gamete fusion

Immediately and only after membrane fusion has occurred, CD9 density started to decrease from the sperm/egg interface (Figure 1B). A spot depleted from CD9 suddenly appears and spreads radially over the gamete interface (Figure 2B; Supplementary Figures S1A and S2A). Subsequently to this local CD9 exclusion process, the amount of CD9 on the whole oolemma suddenly collapsed (Figure 1C). The simultaneous massive increase of EGFP fluorescent signal in the medium surrounding the oocyte into the microfluidic chip (Figures 1D and 2C; Supplementary Figures S1B and S2B) indicated that this collapse was corresponding to a release and not to an internalization. Simultaneously to CD9 release, a nascent egg membrane wave appeared at the extremity of the sperm head (Figure 4). This wave progressively amplified above it up to fully engulf the spermatozoon head that became internalized. Around 25 min were necessary for the full completion of this engulfment process. Finally, the membrane excess resulting from the wave budded to form micrometre size vesicles that detached from the egg membrane at the level of gamete fusion place (Figure 4 and Supplementary Figure S2C).

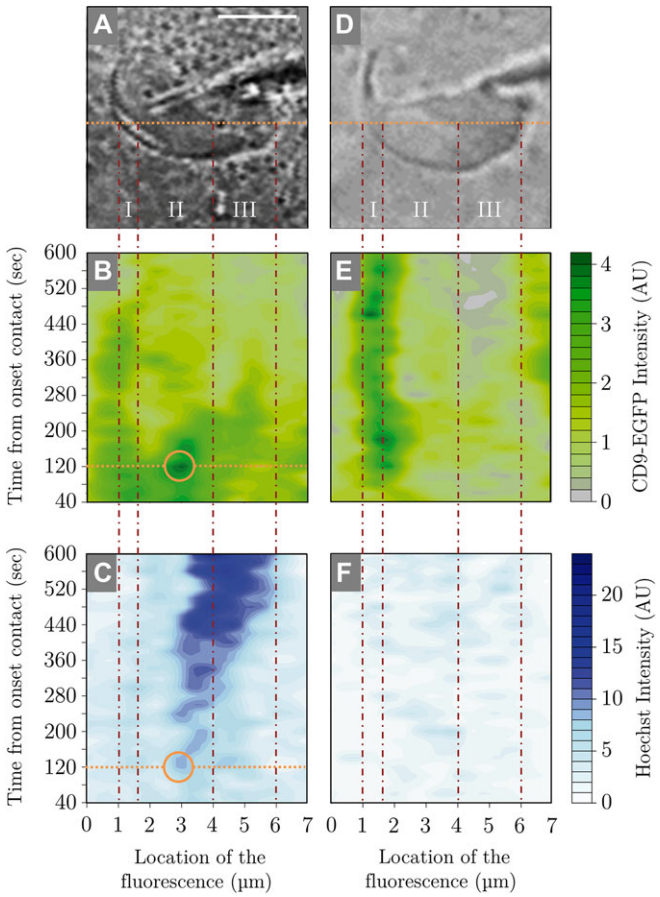

Figure 3 CD9-EGFP and Hoechst spatiotemporal maps during IIVF assays with spermatozoa from Group 3. (**A** and **D**) Three regions of the sperm head: (i) post-acrosomal, (ii) equatorial, and (iii) post-equatorial. The horizontal line crossing these three regions is chosen as region of interest for the construction of the spatiotemporal maps. (**B** and **C**) CD9-EGFP spatiotemporal evolution leading to successful fusion (**B**) and associated spatiotemporal evolution of Hoechst transfer from egg to sperm (**C**). The nucleation of a CD9-rich platform in the sperm equatorial region coincides both in time and place with the apparition of Hoechst signal (orange circles). (**E** and **F**) CD9-EGFP spatiotemporal evolution in the only case for which CD9 concentration took place but not fusion (**E**) and associated absence of Hoechst transfer (**F**).

Discussion

This study provides an unprecedented timeline of the topological and CD9 remodellings of the egg membrane taking place during the early phases of fertilization (Figure 5). Within this timeline, we can distinguish (i) the CD9 membrane events occurring throughout the sperm/egg interaction phase to locally prepare the egg membrane to fuse, (ii) the CD9 membrane processes that follow the fusion reaction, and (iii) the topological egg membrane remodelling leading to the sperm engulfment.

Regarding the sperm/egg interaction period, we demonstrated the causal link between the up and down oscillations of the sperm head on the egg membrane and a spatiotemporal evolution of egg CD9 in the interaction zone that controls gamete fusion. It is not clear whether this remodelling may result from a biochemical response of the egg to the sperm oscillations (mechanotransduction process) or it is a more direct consequence of the sperm movement. The latter hypothesis should be consistent with a mechanism of CD9 densification controlled by an Izumo1/Juno-mediated intercellular adhesion, like the one reported at the interface of eggs and somatic cells transfected with Izumo1 (Chalbi et al., 2014). Each oscillation of the sperm head on the underlying egg microvilli would increase the effective egg surface explored by the sperm and, therefore, maximize the probability of Izumo1/Juno association leading to CD9 remodelling. Consistent with this scenario, Juno antibody reported to prevent Izumo1/Juno association (Chalbi et al., 2014) was also shown to prevent the remodelling of CD9 at the sperm/egg interface (Table 1).

The CD9 remodelling that takes place during the full period of sperm oscillation on the egg membrane (2–3 min) consists in an increase of CD9 amount over the entire interface with the sperm head and to a progressive gathering of CD9 at the level of the sperm equatorial segment up to the nucleation of a CD9-dense platform on which gamete fusion is immediately initiated (Figure 5). How does such a CD9 densification make the egg membrane suitable for fusion is an open question. CD9 amount is suspected to control microvilli curvature (Runge et al., 2007; Zylkiewicz et al., 2010), a parameter determinant for membrane fusion. CD9 is also involved in nanodomains gathering several sperm receptors on which the sperm can strongly adhere (Jegou et al., 2011). According to these features, an increase of CD9 in the sperm/egg interface should result in a gathering of these adhesive nanodomains and, therefore, in a closer sperm and egg membrane apposition, but also to a reshaping of the microvilli adequate for fusion. The fact that fusion failed when the CD9-dense platform was not facing the sperm equatorial segment is consistent with electron micrographs showing that fusion takes place on the equatorial segment (Yanagimachi and Noda, 1970; Bedford et al., 1979; Yanagimachi, 1994). It is also consistent with the absence of fusion between egg and somatic cells transfected with Izumo1 (Inoue et al., 2013, 2015; Chalbi et al., 2014). Last but not least, it points out the requirement of one or several not yet identified specific factors of the sperm equatorial region that would make this region suitable for fusion.

Immediately after fusion, CD9 starts to leave the contact zone. Within <2 min, the equatorial and post-acrosomal zones of the sperm/egg interface get depleted from CD9, and a few minutes after fusion the withdrawal of CD9 from the entire contact zone is complete. This process does not only concern egg CD9 but also sperm Izumo1 which was shown to display the same withdrawal dynamics after fusion (Satouh et al., 2012). As for Juno, it was reported to be enriched at the interface of egg and acrosome-reacted sperm before fusion, but absent from the interface of cells fixed at 40 min after fusion (Inoue et al., 2015). Even if the membrane kinetics of this molecule is missing, we can suspect that Juno is also involved in the same withdrawal process

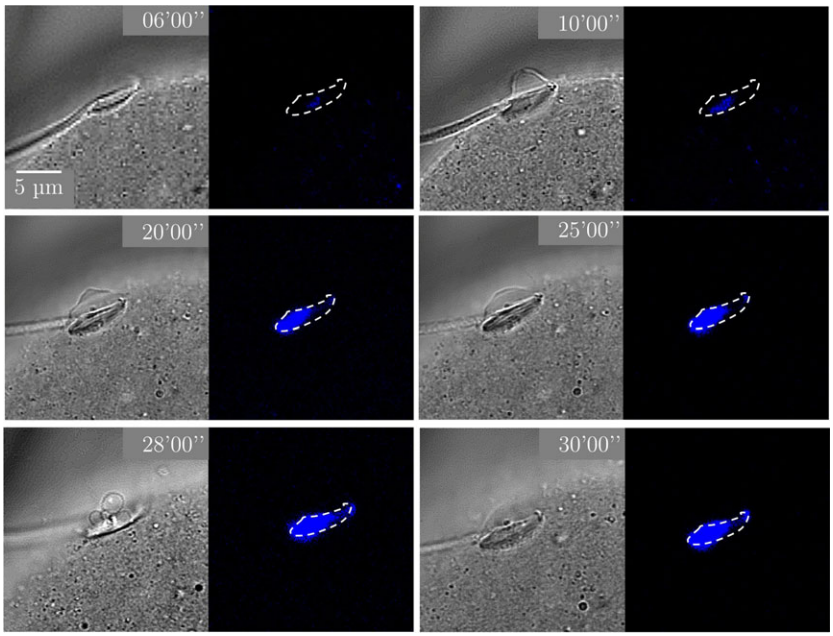

Figure 4 Topological remodelling of the egg membrane for sperm engulfment and vesicle budding process. Simultaneous visualization of topological membrane remodelling leading to sperm engulfment (bright field images) and Hoechst transfer to the sperm DNA (fluorescent images). The timer gives the time from the onset of the gamete contact. Six minutes after contact (~4 min after fusion), the sperm head starts to be engulfed by an egg membrane wave that spreads over it. When the engulfment is complete (here at 25 min), the excess of membrane buds in micro-sized vesicles (28 min) and they detach (30 min). The spreading of Hoechst spot in the sperm DNA indicates that gamete fusion has occurred and that fertilization is still going on.

as CD9 and Izumo1. Moreover, this process may not be limited to these three key proteins. Indeed, a large area surrounding the sperm entry point was reported to be also devoid of the integrin α6β1 after fusion (Ziyyat et al., 2006). After fusion reaction, the oocyte has to integrate the paternal genome and to promptly protect itself against polyspermy. The proteins that were necessary to bring the membranes in close contact and control fusion may become detrimental to the internalization of the sperm. The withdrawal from the sperm entry zone of CD9 and other proteins required for sperm/egg adhesion and fusion is, therefore, likely to favour sperm engulfment but also to make this egg zone fully refractory to any interaction with a new sperm.

A few minutes after fusion, concomitantly to the beginning of the sperm engulfment, a sudden release of CD9 from the whole egg membrane takes place. This release results in a membrane decrease of more than 50% of its CD9 amount within <2 min and in a concomitant transient EGFP fluorescent wave, leaving the egg membrane and propagating into the egg surrounding medium. Owing to the transmembrane structure of CD9, these fluorescent dots are likely to correspond to small egg membrane vesicles carrying CD9, but also other egg membrane proteins among which Juno and other sperm receptors. Since they are not visible on bright field images, their size is likely submicrometric. Interestingly, Juno which is highly expressed on unfertilized eggs, was reported to be barely detectable on the membrane of eggs imaged approximately 1 h after fusion but was found to be redistributed to submicrometric vesicles in the perivitelline space (Bianchi et al., 2014). Unlike CD9, the kinetics of the release of Juno is unknown. However, the similarities of both membrane and vesicles features obtained for CD9 and Juno suggest that the release of these molecules proceeds from a single process taking place only a few minutes after fusion. These vesicles may correspond to exosomes. The latter are small membrane vesicles of endocytic origin, decorated with tetraspanins among which CD9 (Zoller, 2009) and released from many different cells (Thery et al., 2002). They are thought to play a role in transferring materials from cell to cell (Bobrie et al., 2011) including from egg to sperm (Miyado et al., 2008; Barraud-Lange et al., 2012). Here, we show that in the short period of time following fusion, this release process considerably reduces the membrane amount of CD9 and probably other egg proteins involved in gamete adhesion and fusion while it fills the perivitelline space with small vesicles bearing these proteins. The combination of these two features has the potential to efficiently obstruct the fusion of an additional sperm that would have cross the ZP before it becomes fully refractive to sperm penetration (1–2 h for zona hardening) (Inoue and Wolf, 1975). Indeed, because of this fast post-fusion membrane release, such a sperm would have to face two major handicaps: (i) the blockage of its adhesion sites through the binding of the vesicles present in the perivitelline space and (ii) the interaction with an egg altered membrane depleted for proteins essential for gamete adhesion and fusion. Both are consistent with the observed decrease of binding of sperm with fertilized egg plasma membranes (Wolf, 1978; Wolf and Hamada, 1979; Horvath et al., 1993).

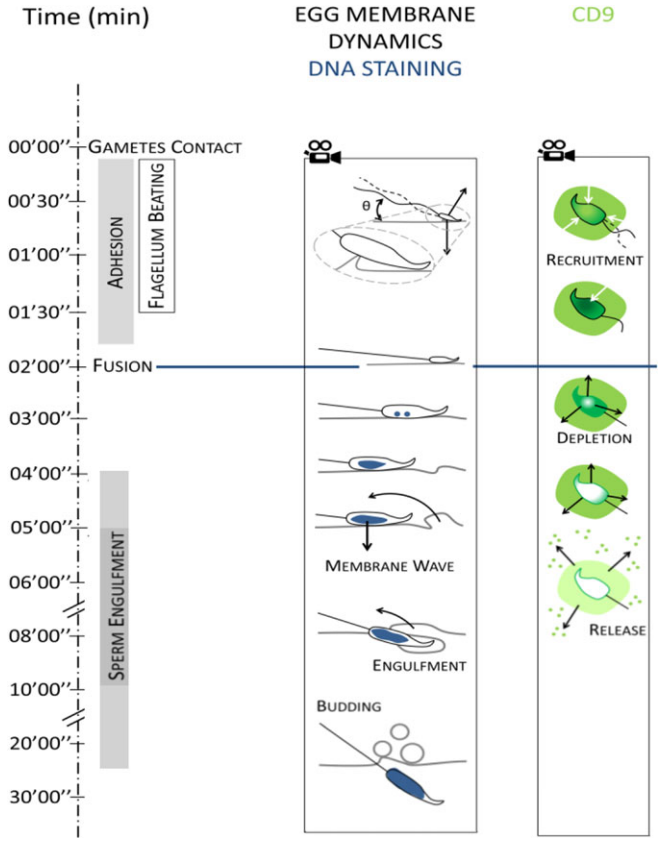

Figure 5 Timeline of the topological and CD9 remodellings of the egg membrane during the early stages of fertilization triggered by specific flagellum beating. Oscillations of the sperm head on the egg membrane (~20°, 1 oscillation/second) trigger CD9 densification at the sperm/egg interface leading in a few dozens of seconds to CD9-dense platforms. Fusion reaction strictly coincides in space and time with the nucleation of the first CD9-rich platform that specifically faces the sperm equatorial segment. Immediately after fusion, CD9 leaves the contact zone, followed within a few minutes by the sudden release of more than 50% of CD9 from the whole oolemma in a process susceptible to contribute to a polyspermy block. Meantime, an egg membrane wave starts to spread above the sperm head and progressively engulfs it. When sperm engulfment is complete, membrane excess buds from the fusion place and detaches as a few micrometre-sized vesicles.

Sperm engulfment starts as soon as the protein withdrawal process from the sperm/egg entry zone is complete. It results in an egg membrane wave that slowly spreads over the sperm and ends up engulfing it 20 min later. Electron microscopy has provided images of such a membrane wave with much better spatial resolution but this technique offers very limited temporal information (Yanagimachi and Noda, 1970). To our knowledge, it is the first time that this phenomenon is observed in real time making possible the determination of its kinetics. It also reveals a transient new budding and release process that takes place as soon as the sperm head is fully internalized (Figure 4, Supplementary Figure S2). It consists in the formation and the detachment of membrane vesicles of a few micrometres. Unlike random blebbing that often indicates the death of the cell in cell culture experiments, these vesicles are spatially localized to the sperm entry point, they are never observed in non-fertilizing cases, and eggs producing these vesicles are healthy since fertilization still proceeds. However, the role of these vesicles remains unclear. They may be a way for the fertilized egg to get rid of the membrane excess reminiscent from the sperm engulfment process.

In conclusion, this unprecedented temporal and spatial accurate view of the sperm/egg interface reveals that gamete fusion is controlled by the achievement of a precise local CD9 densification, itself driven by mechanical constraints due to sperm oscillations. Moreover, the massive release of CD9 that depletes this key protein and their potential partners from the egg membrane within the minutes after fusion is likely to efficiently decrease the gamete fusion ability and, therefore, to limit deleterious polyspermy. By highlighting the necessity to adopt the enlarged viewpoint that the gamete fusion story is an unexpected interplay initiated at the onset of gamete contact between mechanical constraints and proteins, this study represents a conceptual advance in the understanding of the fusion mechanisms in mammal. Last but not least, our microfluidic method paves the way to a systematic study of molecular, membrane, and cortex kinetics for a full understanding of gamete fusion mechanisms and subsequent block to polyspermy and sperm incorporation processes.

Materials and methods

Animals

All animal experimental protocols were approved by the Animal Care and Use Committee Charles Darwin, France (#3254), and Education and Research French Ministry (agreement number APAFIS#3254-2015121712165993 v2). The methods were carried out according to the European Community guideline (Directive 2010/63/EU) on the protection of animals used for scientific purposes.

Sperm

Sperm was obtained from 8 to 10-week-old Acrosin–EGFP male mice (C57Bl6 background). This transgenic mouse line produced from mouse acrosin promoter which expresses EGFP in the sperm acrosome without diminishing fertilizing ability (Nakanishi et al., 1999, 2015). Sperm were expelled from cauda epididymis and vas deferens into Ferticult® IVF medium (Fertipro, France) under mineral oil. Sperm were then incubated in Ferticult® at 37°C, 5% CO_2 in air for 2 h to induce capacitation. After this incubation time, a fraction of sperm has undergone the acrosome reaction. The presence of EGFP in the acrosome facilitates the observation of acrosomal integrity and, therefore, the identification of acrosome-reacted spermatozoa from acrosome intact ones. For experiments, only acrosome-reacted and mobile sperm was selected.

Oocytes

Oocytes were obtained from 6 to 8-week-old CD9-EGFP (Miyado et al., 2008) or CD9KO (Le Naour et al., 2000) female

mice (C57Bl6 background). Female mice were super-ovulated by intraperitoneal injections, first of 5 IU PMSG, followed by 5 IU hCG 48 h apart. Cumulus-intact oocytes were collected into a Ferticult® medium drop 14 h later by tearing the oviduct ampulla from sacrificed mice. CD9KO eggs were used in experiments without additional treatment. CD9-EGFP oocytes were separated from their cumulus by a brief incubation at 37°C, in the presence of hyaluronidase IV-S® (Sigma-Aldrich) (15 mg/ml). Oocytes at metaphase II stage were selected on the basis of the presence of the first polar body. ZP was subsequently removed by rapid treatment with acidic Tyrode's® (Sigma-Aldrich) solution. Eggs were then incubated in Ferticult® for 2 h at 37°C, 5% CO_2 in air. Oocytes were then incubated with Hoechst 33342 (Sigma-Aldrich) at 1 µg/ml for 5 min and washed. For some experiments, CD9-EGFP oocytes were also incubated for 15 min in the presence of Juno antibodies (c = 0.5 µg/ml) and washed. The cells were finally incubated in Ferticult® for at least 1.5 h at 37°C, 5% CO_2 in air before the IIVF experiments.

Individual IIVF in a microfluidic chip

The microfluidic chip is a homemade PDMS 3D-platform extensively described in a previous paper (Ravaux et al., 2016). Briefly, it is composed of an egg-cup to maintain the ZP-free oocyte, whose bottom is opened onto a microfluidic channel that guides an acrosome-reacted sperm to a predefined portion of the oolemma. For IIVF experiments, the chip was filled with M2 medium and placed on the stage of a Leica confocal microscope (Leica SP5-wc2, Leica), equipped with two micromanipulators holding micropipettes. With one micropipette, a ZP-free CD9-EGFP oocyte, preincubated with Hoechst 33342, was positioned in the egg-cup with its amicrovillar part far from the microfluidic channel. With the second pipette, one acrosome-reacted spermatozoon was introduced in the microfluidic channel and let free to interact with the accessible portion of the oocyte. From the onset of sperm/egg contact, the evolution of CD9-EGFP at the egg membrane and the Hoechst transfer from the egg cytoplasm to the fertilizing spermatozoon head were established by time-lapse imaging in bright field and fluorescence, using an oil-immersion objective (HCX PL APO 40 × 1.25 Oil, Leica) and 405 and 488 nm illumination wavelengths. All the measurements were done using the same laser and scanning parameters. Series of six vertical stacks with 1.5 µm increment were recorded at regular time intervals (20–45 sec depending on the experiment) and during 10 min or more, with Leica Application Suite 2.4.1 build 6384. A total thickness of 9 µm was imaged, starting from typically 4.5 µm under the bottom egg membrane, up to a depth of 4.5 µm inside the egg. Images were analysed afterwards with ImageJ from Wayne Rasband, NIH and R software from the R Foundation for Statistical Computing.

For each acquisition time, the six vertical frames were summed with ImageJ. The resulting images were used for fluorescence quantification in Figures 1 and 3. In Figure 2, Supplementary Figures S1 and S2 and Videos S1 and S2, the fluorescent images also correspond to these summed frames, while the images in transmission correspond to the stack on which the sperm head is on best focus.

To build Figure 1A and B, the mean intensities of Hoechst and CD9-EGFP emission were, respectively, measured in a region of interest (ROI) strictly matching the surface of contact between the sperm head and the egg as illustrated in Figure 1E. This ROI was delimitated by drawing a freehand outline of the sperm head surface in contact with the egg (red-dashed line contours in Figure 2, Supplementary Figures S1 and S2). For each time, this operation was repeated five times providing five independent CD9-EGFP mean density values. Each data point of Figure 1A and B corresponds to the average of these five values and the error bars correspond to their standard error. For controls for which no sperm was involved, a ROI equivalent to the previous one (similar contours) was considered and the same quantification was done.

To build Figure 1C, the mean density of egg CD9-EGFP outside the sperm/egg contact area was measured as illustrated in Figure 1E. For each acquisition time, five circular ROI of 5 µm diameter were evenly drawn at the egg membrane, outside the sperm/egg interface, providing five CD9-EGFP mean density values. Each data point of Figure 1C corresponds to the average of these five values and the error bars correspond to their standard error.

To build Figure 1D, the same protocol as in Figure 1C was applied except that the five circular ROI were taken in the medium surrounding the egg and not on the egg membrane.

In Figure 3, the CD9-EGFP and Hoechst spatiotemporal maps were obtained by measuring each pixel intensity on a segment (7 µm, N = 114 pixels) crossing the three regions of the sperm head as illustrated in Figure 3A and D. Then the 114 intensity values obtained for each acquisition time were combined in a 2D array (number of acquisition time rows × 114 lines) with the R software to produce the spatiotemporal maps of Figure 3.

Insemination of CD9KO oocytes with Acr-EGFP sperm

Cumulus from unfertile CD9KO females were inseminated with sperm (10^6 sperm/ml) for 3 h then rinsed. Oocytes with sperm accumulated in the perivitelline space were imaged and the oscillation mode of the spermatozoa in contact with the oolemma was determined.

Supplementary material

Supplementary material is available at *Journal of Molecular Cell Biology* online.

Acknowledgements

We warmly thank Guillaume Dabee, Christophe Auger, and Eleonore Touzalin from IBENS for technical help with mice and Frédéric Pincet, Wladimir Urbach, and Rachid Thiam from LPS ENS, Ahmed Ziyyat from Institut Cochin, Claude Boucheix and Eric Rubinstein from Paris Sud University for fruitful discussions.

Funding

This work was supported by the 'Agence Nationale pour la Recherche' (grant no. ANR-13-BVS5-0004) and the 'Fondation pour

la Recherche Médicale' (fellow grant no. FRM—FDT20150532349 to B.R.).

Conflict of interest: none declared.

References

Barraud-Lange, V., Chalas Boissonnas, C., Serres, C., et al. (2012). Membrane transfer from oocyte to sperm occurs in two CD9-independent ways that do not supply the fertilising ability of Cd9-deleted oocytes. Reproduction *144*, 53–66.

Bedford, J.M., Moore, H.D.M., and Franklin, L.E. (1979). Significance of the equatorial segment of the acrosome of the spermatozoon in Eutherian mammals. Exp. Cell Res. *119*, 119–126.

Bianchi, E., Doe, B., Goulding, D., et al. (2014). Juno is the egg Izumo receptor and is essential for mammalian fertilization. Nature *508*, 483.

Bobrie, A., Colombo, M., Raposo, G., et al. (2011). Exosome secretion: molecular mechanisms and roles in immune responses. Traffic *12*, 1659–1668.

Boucheix, C., and Rubinstein, E. (2001). Tetraspanins. Cell. Mol. Life Sci. *58*, 1189–1205.

Chalbi, M., Barraud-Lange, V., Ravaux, B., et al. (2014). Binding of sperm protein Izumo1 and its egg receptor Juno drives Cd9 accumulation in the intercellular contact area prior to fusion during mammalian fertilization. Development *141*, 3732–3739.

Chernomordik, L.V., Zimmerberg, J., and Kozlov, M.M. (2006). Membranes of the world unite! J. Cell Biol. *175*, 201–207.

Evans, J.P. (2012). Sperm–egg interaction. Annu. Rev. Physiol. *74*, 477–502.

Hemler, M.E. (2005). Tetraspanin functions and associated microdomains. Nat. Rev. Mol. Cell Biol. *6*, 801–811.

Horvath, P.M., Kellom, T., Caulfield, J., et al. (1993). Mechanistic studies of the plasma membrane block to polyspermy in mouse eggs. Mol. Reprod. Dev. *34*, 65–72.

Inoue, N., Hagihara, Y., Wright, D., et al. (2015). Oocyte-triggered dimerization of sperm IZUMO1 promotes sperm–egg fusion in mice. Nat. Commun. *6*, 8858.

Inoue, N., Hamada, D., Kamikubo, H., et al. (2013). Molecular dissection of IZUMO1, a sperm protein essential for sperm–egg fusion. Development *140*, 3221–3229.

Inoue, N., Ikawa, M., Isotani, A., et al. (2005). A novel immunoglobulin superfamily protein, Izumo, is required for sperm to fuse with eggs. Int. J. Androl. *28*, 29–29.

Inoue, M., and Wolf, D.P. (1975). Fertilization-associated changes in the murine zona pellucida: a time sequence study. Biol. Reprod. *13*, 546–551.

Jegou, A., Ziyyat, A., Barraud-Lange, V., et al. (2011). CD9 tetraspanin generates fusion competent sites on the egg membrane for mammalian fertilization. Proc. Natl Acad. Sci. USA *108*, 10946–10951.

Kaji, K., Oda, S., Shikano, T., et al. (2000). The gamete fusion process is defective in eggs of Cd9-deficient mice. Nat. Genet. *24*, 279–282.

Le Naour, F., Rubinstein, E., Jasmin, C., et al. (2000). Severely reduced female fertility in CD9-deficient mice. Science *287*, 319–321.

Miyado, K., Yamada, G., Yamada, S., et al. (2000). Requirement of CD9 on the egg plasma membrane for fertilization. Science *287*, 321–324.

Miyado, K., Yoshida, K., Yamagata, K., et al. (2008). The fusing ability of sperm is bestowed by CD9-containing vesicles released from eggs in mice. Proc. Natl Acad. Sci. USA *105*, 12921–12926.

Nakanishi, T., Ikawa, M., Yamada, S., et al. (1999). Real-time observation of acrosomal dispersal from mouse sperm using GFP as a marker protein. FEBS Lett. *449*, 277–283.

Nakanishi, T., Ikawa, M., Yamada, S., et al. (2015). Corrigendum to "Real-time observation of acrosomal dispersal from mouse sperm using GFP as a marker protein" [FEBS Lett. 449 (1999) 277–283]. FEBS Lett. *589*, 3220.

Ravaux, B., Garroum, N., Perez, E., et al. (2016). A specific flagellum beating mode for inducing fusion in mammalian fertilization and kinetics of sperm internalization. Sci. Rep. *6*, 31886.

Runge, K.E., Evans, J.E., He, Z.Y., et al. (2007). Oocyte CD9 is enriched on the microvillar membrane and required for normal microvillar shape and distribution. Dev. Biol. *304*, 317–325.

Satouh, Y., Inoue, N., Ikawa, M., et al. (2012). Visualization of the moment of mouse sperm-egg fusion and dynamic localization of IZUMO1. J. Cell Sci. *125*, 4985–4990.

Thery, C., Zitvogel, L., and Amigorena, S. (2002). Exosomes: composition, biogenesis and function. Nat. Rev. Immunol. *2*, 569–579.

Wolf, D.P. (1978). The block to sperm penetration in zonal-free mouse eggs. Dev. Biol. *64*, 1–10.

Wolf, D.P., and Hamada, M. (1979). Sperm binding to the mouse egg plasmalemma. Biol. Reprod. *21*, 205–211.

Yanagimachi, R. (1994). Mammalian fertilization. In: Knobil, E., and Neill, J.D. (eds). The Physiology of Reproduction (2nd edn). New York: Raven Press, 189–317.

Yanagimachi, R., and Noda, Y.D. (1970). Electron microscope studies of sperm incorporation into golden hamster egg. Am. J. Anat. *128*, 429–462.

Ziyyat, A., Rubinstein, E., Monier-Gavelle, F., et al. (2006). CD9 controls the formation of clusters that contain tetraspanins and the integrin α6β1, which are involved in human and mouse gamete fusion. J. Cell Sci. *119*, 416–424.

Zoller, M. (2009). Tetraspanins: push and pull in suppressing and promoting metastasis. Nat. Rev. Cancer *9*, 40–55.

Zylkiewicz, E., Nowakowska, J., and Maleszewski, M. (2010). Decrease in CD9 content and reorganization of microvilli may contribute to the oolemma block to sperm penetration during fertilization of mouse oocyte. Zygote *18*, 195–201.